https://doi.org/10.3311/PPee.13453

Periodica Polytechnica Electrical Engineering and Computer Science, 63(3), pp. 191–201, 2019

Accurate Estimation of Frequency-Dependent Losses in High Voltage Test Transformers for the Assessment of Electric Discharge Powers

Kada Laroussi[1*], Samir Flazi[1]

[1] Department of Electrical Engineering, Faculty of Electrical Engineering, University of Science and Technology of Oran Mohamed-Boudiaf, El Mnaouar, BP 1505, Bir El Djir 31000, Oran, Algeria
[*] Corresponding author, e-mail: lavolt@yahoo.fr

Received: 23 November 2018, Accepted: 20 February 2019, Published online: 13 June 2019

Abstract

The work presented in this paper is related to the project GEMUDE (**G**enérateur **M**ultifonction de **D**écharge **E**lectrique) which aims to design a universal high-voltage generator for electrical discharge studies. To design this variable high voltage source that operates in the frequency range of 0 to 1 kHz, the assessment of transformer losses represents a crucial phase during the design process. These losses in the coils and iron core of the transformer are closely related to the frequency and nature of the materials used. This paper presents a comparative study of transformer losses using analytical methods and experimental calorimetry measurements. Steinmetz empirical formula is used to estimate magnetic core losses whereas coil losses are evaluated by solving Maxwell equations. The main goal is to control these losses to limit the internal temperature rise in the transformer through the implementation of an efficient cooling solution. The results obtained by the analytical method were satisfactory which confirm the feasibility of measuring the power absorbed by the various electrical discharge devices upstream of the high-voltage transformer. This is because it turns out that the power of the generator in charge is the total power of the electric discharge and the transformer losses. This method, termed Power Disparity Method (PDM). In this paper, it is an easy and reliable way as compared with high voltage measurement methods.

Keywords

electrical discharge, electric discharge power, high voltage test transformers, multifunction generator, calorimeter

1 Introduction

The design and construction of a multifunction generator for electric discharge tests (GEMUDE project, see Appendix) require a high voltage source with variable frequencies. This source will be used as an example for partial discharge tests [1, 2] carried out at the industrial frequency of 50 Hz. The tests of the cold discharges with dielectric barrier [3] at frequencies are greater than 800 Hz and excimer lamps [4] above 80 kHz, etc.

At present, transformers remain the only technical means that can generate pure sinusoidal high voltages. However, the availability of this type of transformer operating at high frequencies presents a real technical constraint. Since transformer losses are frequency-depend [5-7], excessive heating is generated and, if not dissipated properly, it could damage either the generator itself or cause a failure in the generator's control circuit.

The materials available for either the core or winding of the transformer are usually designed to operate in specific frequency ranges [8, 9] and therefore are not appropriate for our intended design of the universal power source with adjustable frequency. To overcome this constraint, we present in this paper the analytical prediction of the transformer losses which can subsequently be used to design an efficient solution to control the heating in the transformer core and windings.

In the same context, this paper proposes a new method for measuring the power injected into the discharge based on the precise analytical calculation of the losses in the high voltage transformer. This is based on the fact that the power upstream of the transformer would be the power consumed by the discharge plus the losses in the transformer and those in the inductance coils if there are any (Fig. 1). This approach will lead to a considerable simplification of the measuring circuit and improved safety of the system.

The rest of the article is organized as follows: Section 2 presents the classical analytical methods for estimating

Cite this article as: Laroussi, K., Flazi, S. "Accurate Estimation of Frequency-Dependent Losses in High Voltage Test Transformers for the Assessment of Electric Discharge Powers", Periodica Polytechnica Electrical Engineering and Computer Science, 63(3), pp. 191–201, 2019. https://doi.org/10.3311/PPee.13453

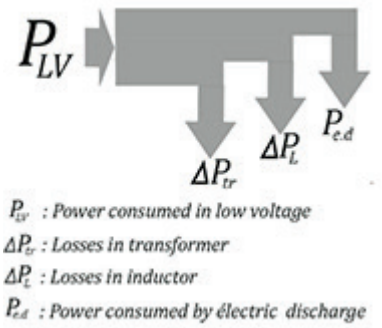

Fig. 1 Power balance of a typical high voltage supply circuit of a discharge.

losses in windings and magnetic cores. Section 3 describes the calorimeter-based experimental setup used for validation of the theoretical results. Section 4 presents the analytical calculation and experimental tests and a comparative study between these results. Section 5 describes an original application of the presented method. Finally, Section 6 will summarize the conclusions on this work.

2 Analytical Approach

2.1 Electric skin effect and losses in windings

2.1.1 General formulation

Losses in transformers are generally modeled based by a lumped element equivalent circuit composed of resistors and inductors. However, to correctly represent a transformer, both resistors and inductors must take into consideration the various physical phenomena that occur inside the core and the windings, such as, the presence of purely resistive losses, hysteresis and Foucault currents. Since these parameters vary with the applied frequency, therefore, a more accurate transformer model should consider the frequency [10-13].

The following analysis is performed on a single turn of the transformer winding. This turn is identical to a cylindrical envelope with an inner radius and an outer radius $b = a + d$, and a length Δl, as shown in Fig. 2. The current distribution produces a magnetic field intensity $H = H_0$ for $r \le a$, and $H = 0$ for $r > a$.

Applying Maxwell's equations to the complex magnetic field intensity gives:

$$\frac{1}{r}\frac{\partial}{\partial r}\left(r\frac{\partial \bar{H}_z}{\partial r}\right) - j\omega\sigma\mu_0\bar{H}_z = 0 \ . \tag{1}$$

The resolution of Eq. (1) leads to the current density as a function of radius.

Because of the symmetry of the cylinder, the magnetic field will consist only of a coaxial component

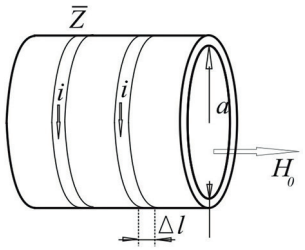

Fig. 2 Single turn model used in the analysis of copper losses.

$$\bar{H}_z = H_z(r) \ . \tag{2}$$

Consider a solution of the form:

$$\bar{H}_z = A_1 J_0(k_1.r) + B_1 K_0(k_2.r) \ . \tag{3}$$

Where J_0 and K_0 are Bessel functions of order 0, and A_1 and B_1 are integration constants, k_1 and k_2 are constant parameters with values: $k_1 = \frac{\sqrt{2}}{\delta} j^{\frac{3}{2}}$ and $k_2 = \frac{\sqrt{2}}{\delta} j^{\frac{1}{2}}$.

Setting the boundary values for Eq. (3), as follows: $H = H_0$ for $r = a$ and $H = 0$ for $r = b$, the coefficients A_1 and B_1 are obtained as:

$$\begin{cases} A_1 = H_0 \dfrac{K_0(k_2.b)}{J_0(k_1a)K_0(k_2b) - J_0(k_1b)K_0(k_2a)} \\ B_1 = -H_0 \dfrac{J_0(k_1.b)}{J_0(k_1a)K_0(k_2b) - J_0(k_1b)K_0(k_2a)} \end{cases} . \tag{4}$$

The current density is determined using the Maxwell equation:

$$\nabla.\bar{H} = j \tag{5}$$

$$j_\varphi = -\frac{\partial \bar{H}_z}{\partial r} \ . \tag{6}$$

Combining Eqs. (1)-(6), the current density can finally be expressed as:

$$\overline{j_\varphi} = A_1 k_1 J_1(k_1.r) + B_1 k_2 K_1(k_2.r) \ . \tag{7}$$

Where J_1 and K_1 are Bessel functions of order 1.

Fig. 3 shows a plot of the current density given by Eq. (6) which reveals the effect of high frequency harmonics on the distribution of current in the coil. It can be observed that the density current increases considerably on the driver's side which is closer to the core, and decreases on the outer side. The unequal distribution of current in the conductor results in an increase in the total resistance of the winding. Thus, two currents of the same amplitude but

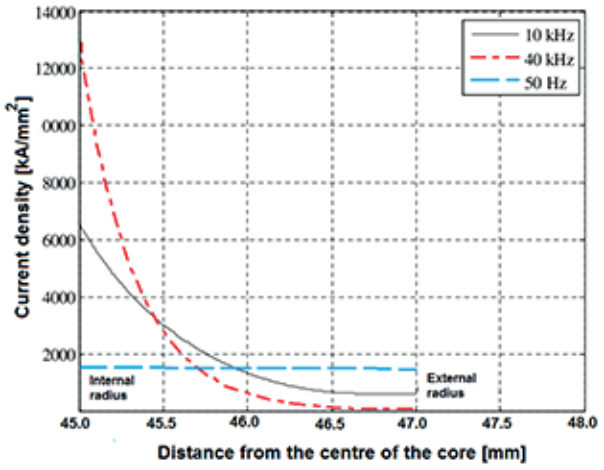

Fig. 3 Current distribution inside a single turn of a coil around circular core at three different frequencies 50 Hz, 10 kHz and 40 kHz when a current of 9 A is flowing in the coil [12].

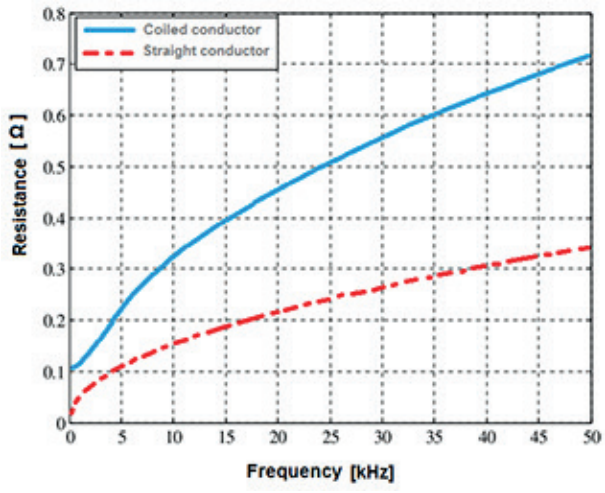

Fig. 4 Increase of the resistance of a conductor due to skin effect for higher frequencies [12].

of different frequency crossing the winding of the transformer will undergo a different resistance and thus generate different levels of losses. The heat developed in the conductor due to the current will be higher closer to the core because of the high density of the current.

The density of ohmic heat losses is determined using Joule's law [11]:

$$P_\sigma = \sigma \left|E_\varphi\right|^2 = \sigma E_\varphi E_\varphi^* = \frac{1}{\sigma}\left|\bar{J}_\varphi\right|^2 . \tag{8}$$

The losses due to Joule heating effect in the volume are given by [11]:

$$P = \int P_\sigma dv = \frac{2\pi\Delta l}{\sigma}\int_{r=a}^{b}\left|\bar{J}_\varphi\right|^2 rdr . \tag{9}$$

Therefore, the resistance R_1 of the envelope is then given by:

$$P = R_1\left|\bar{i}\right|^2 = R_1\left|H_0.\Delta l\right|^2 . \tag{10}$$

By replacing R_1 in Eq. (9) and inserting P from Eq. (10) we can find an expression of winding resistance.

$$R_1 = \frac{\dfrac{2\pi\Delta l}{\sigma}\displaystyle\int_{r=a}^{b}\left|\bar{J}_\varphi\right|^2 rdr}{\left|\bar{i}\right|^2} . \tag{11}$$

Fig. 4 shows how the resistance of the coil increases as the frequency increases. In the region of higher frequencies, the curve appears to flatten and increases approximately at the rate of the square root of the frequency. The resistance of the coil is much greater than that of a straight conductor, since the length and surface of the conductors are equal.

2.1.2 Dowell approximation

Losses in the transformer windings are related to the quasi-static effects that affect the distribution of current density, including the skin effect, proximity effect, edge effect and the effect of iron. As a result, if the magnetic excitation is assumed to be one-dimensional, the increase in the resistance due to the non-homogeneous distribution of current density in the conductor section can be formulated. Conventionally, the increase function F_r is defined as the ratio between the AC resistance and the DC resistance at a given frequency [14]:

$$F_r(X,m) = X\left[\frac{\sinh(2X)+\sin(2X)}{\cosh(2X)-\cos(2X)} + \frac{2(m^2-1)}{3}\frac{\sinh(X)-\sin(X)}{\cosh(X)+\cos(X)}\right] . \tag{12}$$

Where m is the number of layers.

$$X = \frac{h_c}{0.071\sqrt{f}} . \tag{13}$$

Where h_c denotes the thickness of the conductor and f is the frequency of the voltage.

This case is verified when the transformer coils are surrounded by the magnetic circuit, so in the window, is a priori no longer valid outside this window (coil heads) or if there is an air gap in the magnetic core. Fig. 5 shows the increase in the AC resistance as compared to DC resistance for different layers of winding.

The validation of the one-dimensional model (1D) is performed using COMSOL Multi physics [10], proved for the E-type forms of core that the one-dimensional

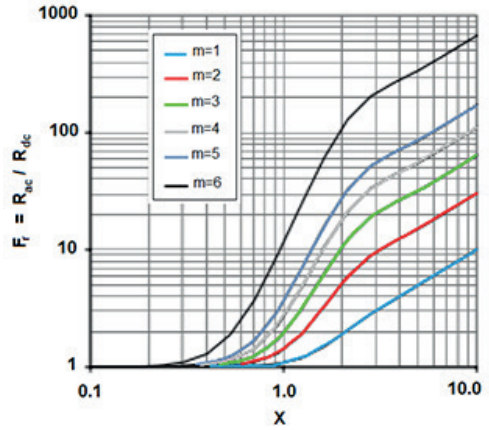

Fig. 5 Resistance factor as a function of X and the number of layers.

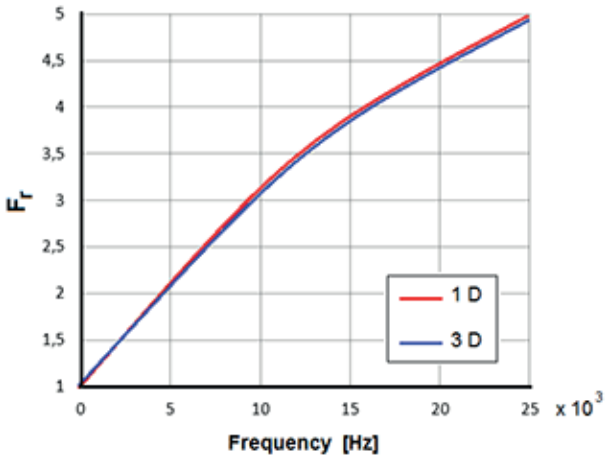

Fig. 6 Comparison between 1D formulation and COMSOL 3D simulation.

formulation is valid for the case where the conductors inside the winding window, and can be easily extended for the case of conductors outside the winding window. Fig. 6 confirms this, since a minimum ratio of 0.96 between the value of the coefficient F_r calculated for the three-dimensional and one-dimensional model can be observed.

The power losses in the windings of the transformer for a current, supplying an electric discharge is then expressed:

$$P_w = R_{dc1} I_{1eff}^2 \frac{1}{m_1} \sum_{n_1=1}^{m_1} \sum_{h=0}^{\infty} F_{r1}(h, f, n_1) \frac{I_{1heff}^2}{I_{1eff}^2} + R_{dc2} I_{2eff}^2 \frac{1}{m_2} \sum_{n_2=1}^{m_2} \sum_{h=0}^{\infty} F_{r2}(h, f, n_2) \frac{I_{2heff}^2}{I_{2eff}^2} \ . \quad (14)$$

Where R_{dc1}, R_{dc2} denote the transformer's primary and secondary resistances respectively, m_1, m_2 represent the number of layers and $F_{r1}(h, f, n_1)$, $F_{r2}(h, f, n_2)$ are the coefficient of increase of resistance for harmonic h and frequency hf.

With the previous one-dimensional model, it is also possible to evaluate the losses in the filter inductance of the supply circuit of the electric discharge cell as a function of the frequency. In some cases, this filtering inductance is very important when certain tests such as partial discharges are performed.

2.2 Losses in the magnetic core

Usually, to estimate losses in ferromagnetic materials, the following empirical formula proposed by Steinmetz [15] is used:

$$P_f = C f^{\alpha} B_m^{\beta} \ . \quad (15)$$

Furthermore, in practice losses in the magnetic core can be divided into three parts: hysteresis losses, Foucault (eddy) current losses and excess losses. Magnetic core losses per unit mass can be calculated by Bertotti formula [16]:

$$P_{f_1} = C_h f B_m^{\alpha} + C_{ci} f^2 B_m^2 + C_{ex} f^{1.5} B_m^{1.5} \ . \quad (16)$$

Where C_h, C_{ci} and C_{ex} are the hysteresis loss, Foucault (eddy) current loss and excess loss coefficients respectively, f is the operating frequency of the transformer, B_m is the maximum density of the magnetic flux of the core and α is an index which depends on the nature of the magnetic material used.

Magnetic materials' manufacturers usually provide models of equations and graphs available to users, which can be easily used to predict and evaluate losses in the volume of the material core. As an example, Fig. 7 represents losses as a function of the magnetic field of certain types of materials commonly used in the manufacture of transformers.

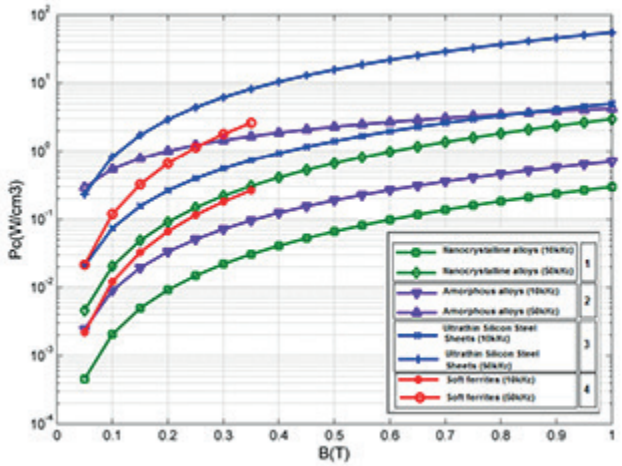

Fig. 7 Loss characteristics based on the flux density [19].

Note that Eq. (15) is valid for the case of a sinusoidal wave form. A second model exists and differs from the previous one in that the dynamic losses are calculated from the temporal evolution of induction [5].

$$P_{f_2} = C_h f B_m^{\alpha} + \frac{C_{ci}}{2\pi^2}\frac{1}{T}\int_0^T \left(\frac{dB}{dt}\right)^2 dt + \frac{C_{exc}}{8764}\frac{1}{T}\int_0^T \left|\frac{dB}{dt}\right|^{1.5} dt \ . \tag{17}$$

The third model is based on the Fourier series decomposition of magnetic induction to take into account the non-sinusoidal excitation in the case of voltage distortion [5].

$$P_{f_3} = C_h \sum_{i=1}^{n} f_n B_{m,n}^{\alpha} + C_{ci} \sum_{i=1}^{n} f_n^2 B_{m,n}^2 + C_{exc} \sum_{i=1}^{n} f_n^{1.5} B_{m,n}^{1.5} \ . \tag{18}$$

Where $B_{m,n}$ and f_n are the amplitude and frequency of the n^{th} harmonic.

Finally, the last model adopted is a combination of the second and third models [17, 15]:

$$P_{f_4} = C_h \sum_{i=1}^{n} f_i B_{m,i}^{\alpha} + \frac{C_{ci}}{2\pi^2}\frac{1}{T}\int_0^T \left(\frac{dB}{dt}\right)^2 dt + \frac{C_{exc}}{8764}\frac{1}{T}\int_0^T \left|\frac{dB}{dt}\right|^{1.5} dt \ . \tag{19}$$

It is worth noting the coefficients in the four models are the same. These coefficients are identified, using the algorithm presented in [18], using both experimental measurements and Eq. (15).

3 Experimental Study

The estimation of power from the measurement of electrical quantities is very complex for transformers working in a wide frequency range because the equivalent series resistance is concealed at low frequencies, by the magnetization inductance and at high frequencies by the leakage inductance and parasitic capacitance. In addition, in high efficiency transformers above 95 %, a low current or voltage measurement error can lead to significant errors in the measurement of losses $(\Delta P > 80\ \%)$. To obtain results with sufficient accuracy, a more reliable measurement method such as calorimetry is used [19].

As mentioned in the introduction, this experimental method is used just to validate the analytical method presented. That is because the use of calorimeter measurements requires measurement periods that can be spread over several days.

3.1 Description of the calorimeter

A hot body exchanges its thermal energy throughout its external surface. Three physical phenomena contribute to this: conduction, convection and radiation [20-23]. Calorimetric measurements used in various electrical engineering applications use this principle to evaluate the errors of a component. The calorimeter thus characterizes the amount of heat exchanged between the sample and the chamber. Several types of calorimeter can be designed examples are: adiabatic, quasi-adiabatic, isothermal, heat flux, etc. Each of these calorimeters has different characteristics. The calorimeter set-up used in this study is shown in Fig. 8 [22, 23].

3.2 Principle of operation

The calorimeter used to measure losses in the transformer has a dual operation mode quasi-adiabatic/isothermal. In the quasi-adiabatic mode, it enables the device under test (DUT) to be placed under controlled heat exchange conditions, i.e. quasi-independent of the outside temperatures and to obtain significant increases in temperature at low injected power [24]. In the isotherm mode, it can absorb the heat generated by the DUT via the exchange of the temperature with external environment. By setting $\Delta T = T_{DST} - T_{ext}$, the thermal leakage can be varied and adapted to the loss levels to be measured. The lower the ΔT is, the lower are the leaks.

The internal walls of the calorimeter are covered with aluminized Mylar sheets to reduce the radiative exchange (ε = 0.05). The internal enclosure is placed on a support of low thermal conductivity $\left(\lambda = 0.35\,\mathrm{Wm^{-1}K^{-1}}\right)$ wearing spikes which reduces further the heat exchanged by conduction. Note that for the quasi-independent mode, a vacuum pump is necessary to limit the convective exchange inside the enclosure.

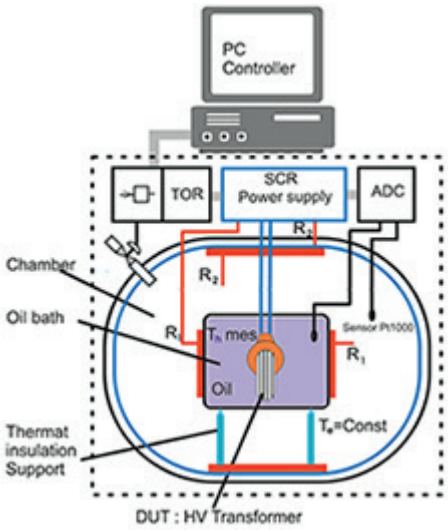

Fig. 8 Simplified diagram of the calorimeter used in this study.

The measurement of losses in isothermal mode is obtained by calculating the difference between the powers injected into the chamber and the enclosure in steady-state after deducing the no-load power losses of the calorimeter [24-26].

The power loss of the DUT is given by:

$$P_d = P_0 - P + \Delta P \ . \tag{20}$$

Where P_0 denotes no-load power of the calorimeter, ΔP is the leakage power of the calorimeter.

4 Losses Evaluation in the Transformer Prototype Used for High Voltage and High Frequency Tests: Analytical Calculation and Experimental Validation

The high voltage transformer model used for the electric discharge tests at different frequencies (YDJZ-5/50) is shown in Fig. 9.

The parameters for this type of transformer are given for two types of magnetic circuits; the first set corresponds to a conventional core (FeSi) for low frequencies made from an alloy of sheet steel and silicon. The second core is of grain-oriented iron-silicon (Fe 3.1 % Si-GO) type. The characteristics of these sheets are shown in Table 1 and the physical dimensions in Fig. 10. With reference to the datasheets of the magnetic circuits, the no-load transformer core losses are evaluated using the following formula:

$$\begin{cases} P_1 = 0.00427.f^{1.53}.B_m^{1.75} \\ P_2 = 0.00362.f^{1.45}.B_m^{1.75} \end{cases} . \tag{21}$$

Fig. 9 Model of the high voltage test transformer used for frequencies ≤ 1 kHz.

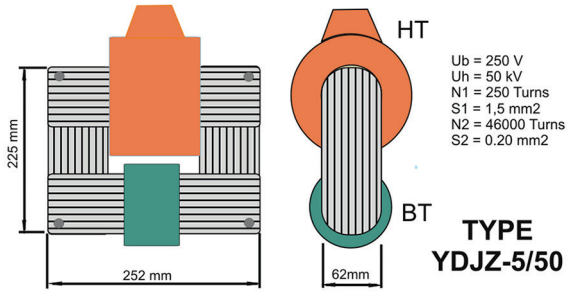

Fig. 10 Physical dimensions and characteristics of the YDJZ-5/50 transformer.

4.1 Excitation by a purely sinusoidal voltage THD ≤ 1 %

4.1.1 Preliminary measurements

A prerequisite to performing experimental measurements is the calibration of the calorimeter to determine the time constant and losses. For instance, if the oil and chamber temperature set points are set to 72.0 °C and 68.2 °C respectively, to have a temperature difference equal to ΔT = 3.8 °C, the power consumption will stabilize at an average value of 49.2 W.

Fig. 11 shows the variation of the absorbed power and Fig. 12 (a) and (b) gives the temperatures of the chamber and the enclosure respectively.

Based on the conditions of the above example, the maximum limit for measuring transformer losses will be 45 W. To obtain the measurements for higher powers, it is necessary to increase the thresholds and facilitate heat elimination towards the outside.

It can be observed that the system reaches the steady-state after about 4 hours of operation. Regarding power leaks, the measurements recorded at no-load given in Table 2 show a conduction coefficient of 13.02 W/°C and a leakage power of 1.2 W.

Table 1 Basic parameters of the high voltage transformer model.

Type of sheet	B_{max} (T)	Tension U_1/U_2 (kV)	Frequency (Hz)	Power (kVA)
0.3 Fe Si	1.2	0.25/50	400	5.0
0.3 FeSi-GO	1.4	0.25/50	1000	5.0

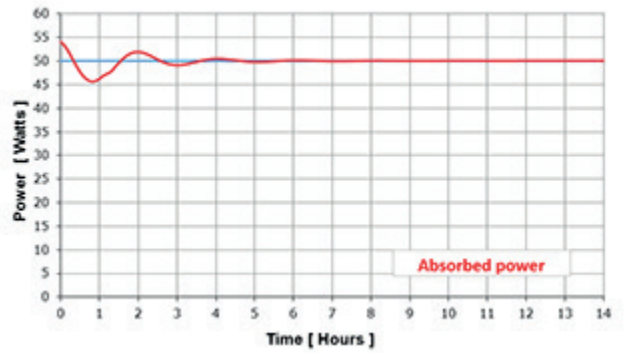

Fig. 11 Absorbed power variation.

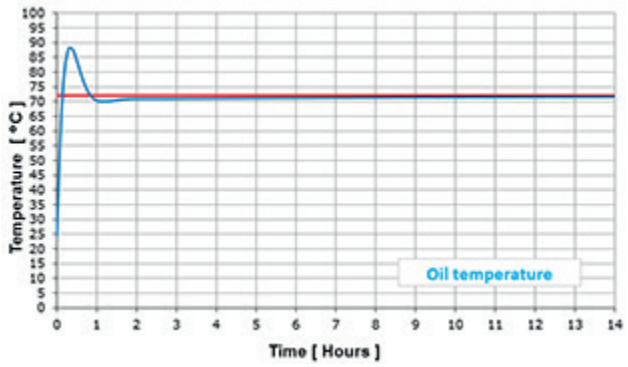

(a)

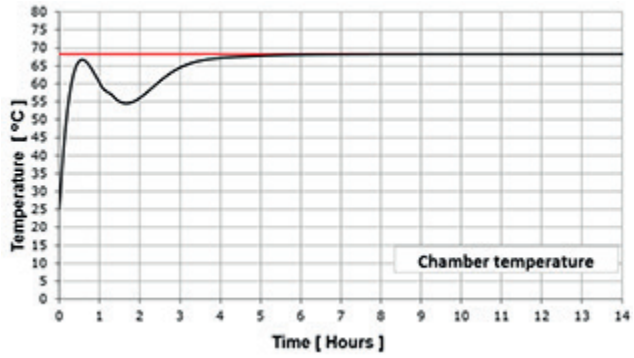

(b)

Fig. 12 Temperatures variation of oil and chamber, (a) oil temperature, (b) chamber temperature.

Table 2 Vacuum power and calorimeter conduction coefficient used.

$T_{chamber}$	T_{oil}	ΔT °C	P W	Coefficient W/°C
68.3	72.0	3.7	49.1	13.27
68.2	72.1	3.9	49.5	12.69
68.2	72.0	3.8	49.2	12.94
68.3	72.0	3.7	48.9	13.21
68.3	72.1	3.8	49.3	12.97

4.1.2 Comparison of the analytical and experimental results

The losses calculated by the analytical method and measured by the calorimeter are shown in Tables 3 and 4 for the first core and Tables 5 and 6 for the second core. It can be seen from Tables 3 and 4 that the errors are small between the calculated and measured losses in the transformer. On the other hand, for the second core FeSi-GO, the differences are clearly important but still acceptable given the empirical model used and the hazards of magnetic sheet manufacturing techniques. It can be noted that the FeSi-GO alloy presents a better performance solution for high frequencies since it gives a loss reduction of 32 % compared to a FeSi core.

Table 3 Losses calculated and measured in the FeSi core.

f [kHz]	P_{f1} calculated [W]	P_{f1} measured [W]	Gap [%]
0.05	2.702	2.8	3.7
0.1	7.802	8.2	5.1
0.15	14.509	15.0	3.5
0.2	22.531	22.0	2.4
0.25	31.700	32.0	0.9
0.3	41.899	43.4	3.6
0.4	65.067	67.1	3.2

Table 4 Electrical losses calculated and measured in the windings.

f [kHz]	P_{f1} calculated [W]	P_{f1} measured [W]	Gap [%]
0.05	45.625	47.2	3.4
0.1	45.884	47.7	4.0
0.15	46.015	48.6	5.6
0.2	46.144	48.6	5.3
0.25	46.274	49.5	6.9
0.3	46.409	50.2	8.2
0.4	46.663	50.7	8.6

Table 5 Losses calculated and measured in the FeSi-GO core for f = 50-1000 Hz.

f [kHz]	P_{f1} calculated [W]	P_{f1} measured [W]	Gap [%]
0.05	2.169	2.2	1.4
0.1	5.927	6.1	2.9
0.2	16.192	16.5	1.9
0.4	44.238	45.4	2.6
0.6	79.639	82.1	3.1
0.8	120.860	124.8	3.3
1.0	167.034	173.7	4.0

Table 6 Electrical losses calculated and measured in the windings for f = 50-1000 Hz

f [kHz]	P_{f1} calculated [W]	P_{f1} measured [W]	Gap [%]
0.05	45.625	47.2	3.4
0.1	45.884	47.7	4.0
0.2	46.144	48.6	5.3
0.4	46.663	50.7	8.6
0.6	47.168	51.4	8.9
0.8	47.681	52.0	9.1
1.0	48.195	52.6	9.1

4.2 Excitation by a rectangular peripheral voltage - THD = 12 %

The tests are performed by injecting a voltage with a rectangular waveform at 50 Hz (Fig. 13) that we analyzed by oscilloscope TEKTRONIX TBS2000. The voltage has the harmonics of 3rd, 5th, 7th, 9th and 11th order as shown in Fig. 14.

The power losses in the windings or in the core can be evaluated by the superposition method of the harmonic components of the supply voltage.

$$P_i = \sum_{1}^{n} P_i\left(f_i, B_{m,i}\right) . \tag{22}$$

The comparison of the total magnetic losses determined from the Bertotti model to those measured on the Fe-Si-GO core plates is illustrated in Fig. 15.

The loss density values obtained experimentally are in good agreement with those obtained with the theoretical models. This is valid up to maximum inductions of the order of 1.2 T. Beyond this, the theoretical curve deviates from the experimental one. This can be explained by the fact that the analytic model does not consider the phase of each harmonic, but only the amplitude and order of the harmonics. Therefore, the iron losses are automatically overestimated.

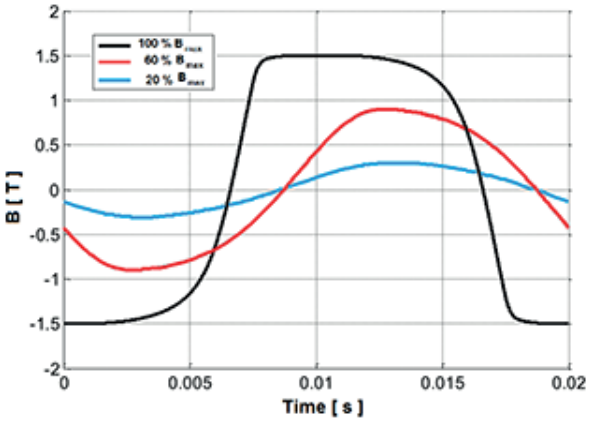

Fig. 13 Evolution of the rectangular supply voltage by the magnetic induction scale.

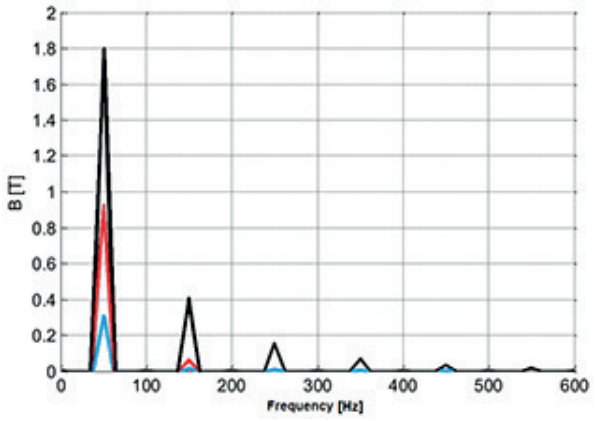

Fig. 14 Frequency spectrum resulting from the Fourier series decomposition of the magnetic induction.

5 Application of the Proposed Method to the Measurement of Electric Discharge Powers

Power measurements in stationary steady-state discharge devices, such as ozone generators or plasma generators in industry, present real difficulties because they require special probes and specific circuits to each measurement. The study presented above shows that the measurement can be moved upstream of the high voltage transformer. Then the discharge power P_{dec} will be determined as the difference between the power upstream of the transformer P_{am} and the losses calculated there in ΔP_{tr} .

$$P_{e.d} = P_{am} - \Delta P_{tr} \tag{23}$$

In our case, the GEMUDE test bench is controlled by PLC (Programmable Logic Controller). The latter has 14 bit analog input units, which makes it possible to measure and record the voltage and current modules at the input of the transformer. Fig. 16 shows the electrical wiring diagram of the different measuring equipment and Fig. 17 presents the flowchart of the program designed to calculate the power of electric discharge.

To assess the accuracy of the proposed method, the power consumed by an ozone production cell, with no characteristics, is measured. Fig. 18 shows the tested ozone generator. The high-voltage side power is measured by air reference of the Lissajous curves [27] plotted by the oscilloscope. The results of the two methods are shown in Fig. 19.

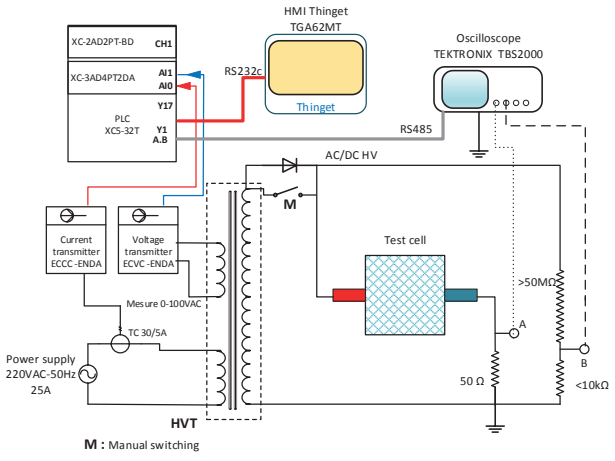

Fig. 16 Electrical diagram of the discharge power measuring circuit.

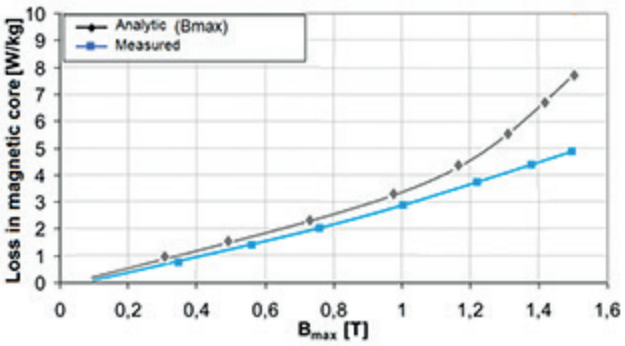

Fig. 15 Comparison of the analytical and experimental models for a rectangular voltage.

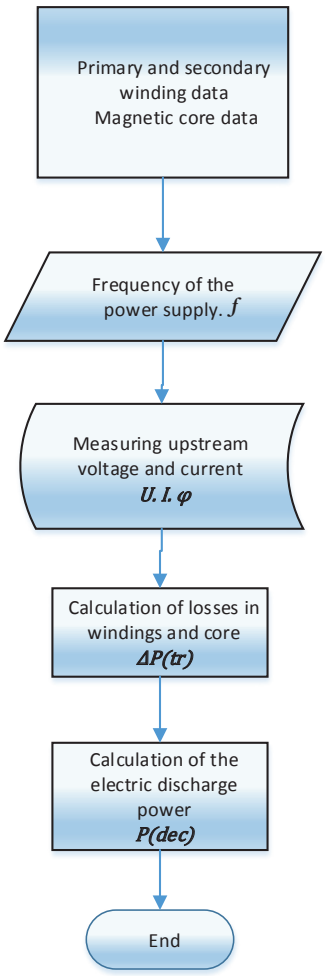

Fig. 17 Flowchart for calculating the discharge power.

It can be seen from the Fig. 19 for low voltage values that there is a significant difference (> 15 %) between the two methods This is partly due to the following cumulative inaccuracies:

- The basic assumptions of approximations of the two methods.
- The characteristics of the magnetic cores used.

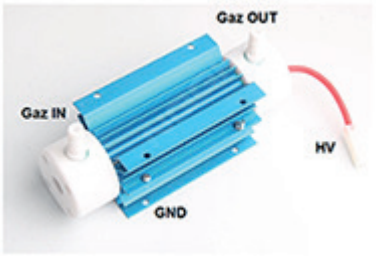

Fig. 18 Ozone generator used for testing.

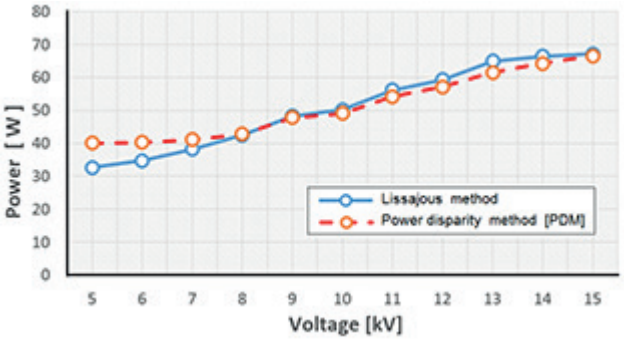

Fig. 19 Power consumed by the ozone generator measured by the Lissajous method and by the proposed PDM.

- The method for estimating the area of Lissajous figures.
- The accuracy of the measuring equipment, which has measurement errors of less than 1.5 %.

On the other hand, the results displayed for other supply voltage (> 6.5 kV), show a good agreement between the two methods. From the remaining graphical representations, it can be observed that the difference remains small between the curves obtained either by the PDM methods or by the classical method of Lissajous [28]. This confirms the feasibility of the PDM method, which makes it possible to have real-time measurements during electrical discharge tests.

6 Conclusion

High voltage transformers intended for electrical discharge studies should be assessed for their use at high frequencies, which may cause active losses and a significant increase in the internal temperature. To overcome this, it is essential to select the appropriate magnetic materials. Alternatively, a cooling circuit operating at threshold can be designed to mitigate overheating. This solution is implemented in the transformer used for the GEMUDE project.

The technical difficulties of evaluating the power of the electric discharges during the experimental studies performed by the test bench GEMUDE have led us to investigating other avenues. The main contribution of this paper is

to develop a new method for measuring the power of electric discharge implemented with the help of the GEMUDE test bench, which has been designed and developed for scientific research and educational demonstrations.

The electric discharge power measurement by the PDM (power disparity method) using GEMUDE test bench gives reasonably good results. Experimental measurements based on the Lissajous curves method confirmed these findings. This confirms the feasibility and reliability of the proposed method for solving a major problem in the field of electrical discharges. The measurement of the power absorbed by the reactors is performed easily in low voltage and upstream of high voltage transformer. This method is safe for both the user and the hardware.

For distorted voltages, it is essential to carry out an FFT (Fast Fourier transform) harmonic analysis, to estimate the overall losses and then to determine the electric discharge power.

References

[1] Tozzi, M. "Partial discharges in power distribution electrical system: pulse propagation models and detection optimization", PhD Thesis, University of Bologna, 2010.

[2] Garcia-Colon, V. R. "Partial discharge measurement during impulse testing", presented at IEEE Conference on Electrical Insulation and Dielectric Phenomena (CEIDP), Des Moines, Iowa, USA, Oct 19, 2014.

[3] Brandenburg, R. "Dielectric barrier discharge: progress on plasma sources and on the understanding of regime and single filaments", Plasma Sources Science and Technology, 26(5), article id 053001, 2017. https://doi.org/10.1088/1361-6595/aa6426

[4] Akashi, H., Oda, A., Sakai, Y. "Development of streamers in dielectric-barrier-discharge excimer lamp", IEEE Transactions on Plasma Science, 36(4), pp. 1336–1337, 2008. https://doi.org/10.1109/TPS.2008.920313

[5] Krings, A., Soulard, J. "Overview and Comparison of Iron Loss Models for Electrical Machines", Journal of Electrical Engineering, 10(3), pp. 163–171, 2010.

[6] Fiorillo, F., Bertotti, G., Appino, C., Pasquale, M. "Soft magnetic materials", In: Webster, J. G. (ed.) Wiley Encyclopedia of Electrical and Electronics Engineering, John Wiley and Sons, USA, 2016. https://doi.org/10.1002/047134608X.W4504.pub2

[7] Mu, M., Li, Q., Gilham, D. J., Lee, F. C., Ngo, K. D. T. "New core loss measurement method for high-frequency magnetic materials", IEEE Transactions on Power Electronics, 29(8), pp. 4374–4381, 2014. https://doi.org/10.1109/TPEL.2013.2286830

[8] Muhlethaler, J., Biela, J., Kolar, J. W., Ecklebe, A. "Improved Core-Loss Calculation for Magnetic Components Employed in Power Electronic Systems", IEEE Transactions on Power Electronics, 27(2), pp. 964–973, 2012. https://doi.org/10.1109/TPEL.2011.2162252

[9] Kulkarni, S. V., Khaparde, S. A. "Magnetic Characteristics", In: Transformer engineering design and practice, Marcel Dekker, Inc., New York, USA, pp. 42–55, 2004.

[10] Monteiro, J. H. A., Coelho, E., Costa, M., Jinno, A., Pinto, G., Kurokawa, S., Mohamed, O., Gatous, O., Pissolato, J. "Simplified skin-effect formulation for power transmission lines", IET Science Measurement and Technology, 8(2), pp. 47–53, 2014. https://doi.org/10.1049/iet-smt.2013.0072

[11] Cozonac, D., Mihaila, V., Vélu, G., Duchesne, S., Lecointe, J. P. "Performance Comparision of Winding Wires for High-Temperature Rotating Machines", In: 2013 IEEE International Conference on Solid Dielectrics (ICSD), Bologna, Italy, 2013, pp. 318–321. https://doi.org/10.1109/ICSD.2013.6619771

[12] Berglund, R. "Frequency Dependence of Transformer Losses", MSc Thesis, Chalmers University of Technology, 2009.

[13] Wang, Y., Zheng, Z. "Research on the winding losses based on finite element method for high frequency transformer", In: International Conference on Engineering Technology and Application (ICETA 2015), HighTatras, Slovakia, 2015, Article Number 02011. https://doi.org/10.1051/matecconf/20152202011

[14] Dowell, P. L. "Effect of eddy currents in transformers windings", Proceedings of the Institution of Electrical Engineers, 113(8), pp. 1387–1394, 1966. https://doi.org/10.1049/piee.1966.0236

[15] Steinmetz, C. P. "On the law of hysteresis", Proceedings of the IEEE, 72(2), pp. 197–221, 1984. https://doi.org/10.1109/PROC.1984.12842

[16] Eggers, D., Steentjes, S., Hameyer, K. "Advanced iron-loss estimation for nonlinear material behavior", IEEE Transactions on Magnetics, 48(11), pp. 3021–3024, 2012. https://doi.org/10.1109/TMAG.2012.2208944

[17] Benabou, A., Leite, J. V., Clénet, S., Simão, C., Sadowski, N. "Minor loops modelling with a modified Jiles–Atherton model and comparison with the Preisach model", Journal of Magnetism and Magnetic Materials, 320(20), pp 1034–1038, 2008. https://doi.org/10.1016/j.jmmm.2008.04.092

[18] Simao, C., Sadowski, N., Batistela, N. J., Bastos, J. P. A. "Evaluation of Hysteresis Losses in Iron Sheets Under DC-biased Inductions", IEEE Transactions on Magnetics, 45(3), pp. 1158–1161, 2009. https://doi.org/10.1109/TMAG.2009.2012663

[19] Lei, G., Zhu, J., Guo, Y. "Multidisciplinary Design Optimization Methods for Electrical Machines and Drive Systems", 1st ed., Springer, Berlin, Heidelberg, Germany, 2016. https://doi.org/10.1007/978-3-662-49271-0

[20] Cao, W., Bradley, K. J., Ferrah, A. "Development of a high-precision calorimeter for measuring power loss in electrical machines", IEEE Transactions on Instrumentation and Measurement, 58(3), pp. 570–577, 2009. https://doi.org/10.1109/TIM.2008.2005083

[21] Keradec, J. P. "Validating the Power Loss Model of a Transformer by Measurement: Difficult but Essential", IEEE Industry Applications Magazine, 13(4), pp. 42–48, 2007. https://doi.org/10.1109/MIA.2007.4283508

[22] Cao, W., Asher, G. M., Huang, X., Zhang, H., French, I., Zhang, J., Short, M. "Calorimeters and techniques used for power loss measurements in electrical machines", IEEE Instrumentation & Measurement Magazine, 13(6), pp. 26–33, 2010. https://doi.org/10.1109/MIM.2010.5669610

[23] Amaya, J. "Unsteady coupled convection, conduction and radiation simulations on parallel architectures for combustion applications", PhD Thesis, National Polytechnic Institute of Toulouse, 2010. [online] Available at: https://tel.archives-ouvertes.fr/tel-00554889 [Accessed: 14 June 2018]

[24] Christen, D., Badstuebner, U., Biela, J., Kolar, J. W. "Calorimetric Power Loss Measurement for Highly Efficient Converters", In: The 2010 International Power Electronics Conference-ECCE ASIA, Sapporo, Japan, 2010, pp. 1438–1445. https://doi.org/10.1109/IPEC.2010.5544503

[25] Obame Ndong, E. "Développement d'un dispositif de calorimétrie par rayonnement thermique: application à la mesure des pertes dans les composants électriques" (Development of a thermal radiation calorimetry device: application to the measurement of losses in electrical components), PhD Dissertation, University of Grenoble, 2010. [online] Available at: https://tel.archives-ouvertes.fr/tel-00523756 [Accessed: 12 June 2018] (in French)

[26] Mc Duff, G. G., Rust, K. R. "Calorimetric measurement of equivalent series resistance of low-loss, high repetition rate pulse discharge capacitors", In: Proceedings of the 17th IEEE Power Modulator Symposium, Seattle, USA, 1986, pp. 202–206.

[27] Biganzoli, I., Barni, R., Gurioli, A., Pertile, R., Riccardi, C. "Experimental investigation of Lissajous figure shapes in planar and surface dielectric barrier discharges", Journal of Physics: Conference Series, 550, article ID: 012039, 2014. https://doi.org/10.1088/1742-6596/550/1/012039

[28] Holub, M. "On the measurement of plasma power in atmospheric pressure DBD plasma reactors", International Journal of Applied Electromagnetics and Mechanics, 39, pp. 81–87, 2012. https://doi.org/10.3233/JAE-2012-1446

Appendix

GEMUDE project: This project was initiated at LGEO research laboratory (University of Science and technology of Oran, Algeria) and is for the design and development of a Multifunction Generator of Electric Discharge; specifically for research on electric discharge and its applications. It is also used to run some demonstrations for electrical engineering students.